J. Fluid Mech. (2007), *vol.* 570, *pp.* 47–67. © 2007 Cambridge University Press
doi:10.1017/S0022112006002904 Printed in the United Kingdom

Equatorial wave attractors and inertial oscillations

By LEO R. M. MAAS AND UWE HARLANDER

Royal Netherlands Institute for Sea Research, P.O. Box 59, 1790 AB Texel, The Netherlands

(Received 5 April 2005 and in revised form 9 June 2006)

Three different approximations to the axisymmetric small-disturbance dynamics of a uniformly rotating thin spherical shell are studied for the equatorial region assuming time-harmonic motion. The first is the standard β-plane model. The second is Stern's (*Tellus*, vol. 15, 1963, p. 246) homogeneous, equatorial β-plane model of inertial waves (that includes all Coriolis terms). The third is a version of Stern's equation extended to include uniform stratification. It is recalled that the boundary value problem (BVP) that governs the streamfunction of zonally symmetric waves in the meridional plane becomes separable only for special geometries. These separable BVPs allow us to make a connection between the streamfunction field and the underlying geometry of characteristics of the governing equation. In these cases characteristics are each seen to trace a purely periodic path. For most geometries, however, the BVP is non-separable and characteristics and therefore wave energy converge towards a limit cycle, referred to as an equatorial wave attractor. For Stern's model we compute exact solutions for wave attractor regimes. These solutions show that wave attractors correspond to singularities in the velocity field, indicating an infinite magnification of kinetic energy density along the attractor. The instability that arises occurs without the necessity of any ambient shear flow and is referred to as geometric instability.

For application to ocean and atmosphere, Stern's model is extended to include uniform stratification. Owing to the stratification, characteristics are trapped near the equator by turning surfaces. Characteristics approach either equatorial wave attractors, or point attractors situated at the intersections of turning surfaces and the bottom. At these locations, trapped inertia–gravity waves are perceived as near-inertial oscillations. It is shown that trapping of inertia–gravity waves occurs for any monochromatic frequency within the allowed range, while equatorial wave attractors exist in a denumerable, infinite set of finite-sized continuous frequency intervals. It is also shown that the separable Stern equation, obtained as an approximate equation for waves in a homogeneous fluid confined to the equatorial part of a spherical shell, gives an exact description for buoyancy waves in uniformly but radially stratified fluids in such shells.

1. Introduction

An important property of the equatorial region is that it acts as a waveguide, trapping disturbances in the vicinity of the equator. The classical trapped waves are found as eigensolutions of the Laplace tidal equations under certain boundary conditions. To simplify their description, these modes have also been computed for the equatorial β-plane with a flat surface and bottom (Matsuno 1966). For the same geometry and under the same approximations, similar solutions can also be found for a uniformly stratified fluid. We notice that in such a traditional description

https://doi.org/10.1017/S0022112006002904 Published online by Cambridge University Press

inertia–gravity waves, travelling in the meridional plane, reflect symmetrically from boundaries and turning surfaces. Despite the fact that the wave field's spatial structure is governed by a hyperbolic equation, by virtue of this special symmetric orientation of the boundaries a discrete set of eigenfrequencies and smooth eigenmodes is found. This is similar to elliptic interior problems, e.g. encountered in acoustics or quantum mechanics (Nedelec 2001). However, equatorial wave eigenspectra appear to be infinitely degenerate and dense (Høiland 1962) and as such differ strongly from the isolated and non-degenerate spectra of elliptic problems. As will be demonstrated here, the discreteness of the spectrum and smoothness of the eigenmodes is also lost when the symmetry in boundary orientation is broken. In an inviscid description, one generically obtains continuous spectra and singular solutions.

Sections 2–4 address the existence of such continuous frequency bands and demonstrate that wave attractors are quite common in geometries used in connection with zonally symmetric equatorial wave problems. Like critical level singularities in shear flows, wave attractor singularities are dynamically important since locally they might lead to mixing and to wave–mean flow interactions (Maas 2001). Although most of the theoretical results have been known for over thirty years (Stern 1963; Bretherton 1964; Stewartson 1971, 1972; Israeli 1972) they seem to have been considered as special phenomena of pure inertial waves with limited relevance for stratified fluids like the oceans or the atmosphere. Therefore, in §§5 and 6, we focus on new aspects that arise when stratification is introduced and gravity becomes important. We speculate on possible observational evidence for the existence of wave attractors in oceans and atmospheres. We end by arguing that the singular nature of wave attractors presents a kind of geometric instability. This shows that all kinds of classically stable flow configurations are, in fact, locally unstable to infinitesimal perturbations when confined to a symmetry-breaking geometry.

2. Governing equations

We consider linear monochromatic waves of frequency σ, confined to a uniformly stratified layer of fluid between a flat bottom ($z=0$) and surface ($z=H$), employing the Boussinesq approximation on the equatorial β-plane. These waves are governed by (Gill 1982)

$$\mathrm{i}\sigma u + 2\Omega w - \beta y v = -p_x, \tag{2.1}$$

$$\mathrm{i}\sigma v + \beta y u = -p_y, \tag{2.2}$$

$$\mathrm{i}\sigma w - 2\Omega u = -p_z + b, \tag{2.3}$$

$$\mathrm{i}\sigma b + w N^2 = 0, \tag{2.4}$$

$$u_x + v_y + w_z = 0. \tag{2.5}$$

Here equatorial β is defined as

$$\beta = \frac{2\Omega}{R}, \tag{2.6}$$

where Ω and R are the angular frequency ($7.292 \times 10^{-5}\,\mathrm{s}^{-1}$) and radius ($6371 \times 10^{3}\,\mathrm{m}$) of the Earth. With these values $\beta \approx 2.3 \times 10^{-11}\,\mathrm{m}^{-1}\,\mathrm{s}^{-1}$. These linearized equations represent conservation equations of momentum and buoyancy in an incompressible fluid. Vector (u, v, w) represents velocity components in the zonal, meridional and vertical (x, y, z) directions, respectively. The modified pressure p is the reduced pressure divided by the constant reference density $\bar{\rho}$. The total density is composed of

https://doi.org/10.1017/S0022112006002904 Published online by Cambridge University Press

this reference density plus the static, vertically varying part, $\rho_0(z)$, plus the spatio-temporally varying part ρ, which are of successively smaller magnitude. Buoyancy is defined as $b=-g\rho/\bar{\rho}$ and buoyancy frequency $N=(-g\bar{\rho}^{-1}\,\mathrm{d}\rho_0/\mathrm{d}z)^{1/2}$, which is assumed constant here. We employ scaling $[x, z, \sigma, u, w, p, b]=(L, H, NH/L, U, HU/L, NHU, NU)$, with U a horizontal velocity scale, $L=(NH/\beta)^{1/2}$ a horizontal length scale, in which ocean depth scale H is of order 4000 m. For $N=10^{-3}\,\mathrm{s}^{-1}$, L is of order 400 km. Scales in the y-direction are taken as similar to those in x-direction. The momentum and buoyancy equations thus reduce to

$$\mathrm{i}\sigma u+\frac{2\Omega}{N}w-yv=-p_x, \tag{2.7}$$

$$\mathrm{i}\sigma v+yu=-p_y, \tag{2.8}$$

$$\mathrm{i}\left(\frac{H}{L}\right)^2\sigma w-\frac{2\Omega}{N}u=-p_z+b, \tag{2.9}$$

$$\mathrm{i}\sigma b+w=0. \tag{2.10}$$

The incompressibility condition is unchanged. Notice that the frequency scale, $NH/L=(NH\beta)^{1/2}\approx 10^{-5}\,\mathrm{s}^{-1}$, is somewhat below the Earth's rotation frequency Ω.

In the following we employ three approximations. They are intended to simplify the problem as much as possible without losing the essence. The models describe linear trapped zonally symmetric monochromatic inertial and inertia–gravity waves, confined to homogeneous (§§ 3 and 4) or uniformly stratified (§ 5) layers of fluid on the equatorial β-plane.

3. Standard equation

Let us first illustrate that smooth eigenmodes and symmetrically reflecting characteristics are two different sides of the same coin. Symmetrical (Snellian) reflections from surface/bottom boundaries and turning surfaces can occur for a very limited set of boundary geometries only, which can therefore be considered as rare exceptions. Here we demonstrate this by a deformation of the lower boundary which immediately leads to converging characteristics, i.e. to a situation where smooth eigenmodes cannot exist.

It is well-known that (2.7)–(2.9), applied to a fluid layer with a flat surface and bottom, possess a discrete spectrum when the so-called traditional and hydrostatic approximations are made (Bretherton 1964; Matsuno 1966). The traditional approximation consists of neglecting terms in (2.7) and (2.9) preceded by the parameter $2\Omega/N$, considering this to be small (a questionable assumption in the deeper parts of the ocean). This conforms with the neglect of the tangential projection of the Earth's rotation vector. The second assumption under which a discrete spectrum is found is concerned with the neglect of the vertical acceleration, the first term in (2.9), based on the assumption that also $(H/L)^2\ll 1$. Since later on we will look basically at zonally symmetric waves, we will additionally assume axisymmetry ($\partial_x=0$). Together these assumptions lead to

$$\mathrm{i}\sigma u-yv=0, \tag{3.1}$$

$$\mathrm{i}\sigma v+yu=-p_y, \tag{3.2}$$

$$0=-p_z+b, \tag{3.3}$$

$$i\sigma b+w=0, \tag{3.4}$$

$$v_y+w_z=0. \tag{3.5}$$

https://doi.org/10.1017/S0022112006002904 Published online by Cambridge University Press

With the introduction of a meridional streamfunction ψ the spatial structure of the streamfunction field is determined by the standard equation

$$\psi_{yy} - (\sigma^2 - y^2)\psi_{zz} = 0. \tag{3.6}$$

This has to be solved subject to the requirements that $\psi = 0$ at the bottom ($z = 0$) and surface ($z = 1$), and $\psi \to 0$ for $|y| \to \infty$. Not only is the equation separable, $\psi = \sum \psi_n(y) \sin(n\pi z)$, with n a non-negative integer, but also each of these vertical modes satisfies the top and bottom boundary condition separately. The resulting meridional structure for $\psi_n(y)$ is determined by Weber's equation (Merzbacher 1970)

$$\frac{\mathrm{d}^2\psi_n}{\mathrm{d}y'^2} + (E - y'^2)\psi_n = 0, \tag{3.7}$$

where $y' = y(n\pi)^{1/2}$ and $E = n\pi\sigma^2$. This equation also governs the behaviour of a classical linear harmonic oscillator. With $\psi_n = \exp(-y'^2/2)\phi_n$ this yields

$$\frac{\mathrm{d}^2\phi_n}{\mathrm{d}y'^2} - 2y'\frac{\mathrm{d}\phi_n}{\mathrm{d}y'} + (E - 1)\phi_n = 0. \tag{3.8}$$

Solutions for which ψ_n vanishes for large $|y'|$ are given by Hermite polynomials $H_m(y')$, provided $E = 2m + 1$, for integer m. This determines a further quantization of the frequency. From the definition of E, solutions

$$\psi \sim \exp(-n\pi y^2/2) H_m\big((n\pi)^{1/2} y\big) \sin(n\pi z) \tag{3.9}$$

thus exist for frequencies σ determined by

$$\sigma_{mn} = \pm\left(\frac{2m+1}{n\pi}\right)^{1/2}. \tag{3.10}$$

This expression for the eigenfrequencies is remarkable for two reasons. First, the eigenfrequencies are dense: any arbitrary value of $\sigma_{mn}^2\pi$ is arbitrarily closely to a rational frequency p/q (p and q co-prime), which itself can be approximated arbitrarily closely by a ratio of the form obtained on quantization: $(2m + 1)/n$. Second, these frequencies are degenerate: multiple spatial structures (counted below by integer j), belong to the same frequency as can be observed from the invariance of $\pi\sigma_{mn}^2 = (2m + 1)/n$, equal to p/q, say, under transformation $m = (p - 1)/2 + p(j - 1)$ and $n = q(2j - 1)$. These two properties are like those encountered for internal waves (Høiland 1962; Münnich 1993; Maas & Lam 1995) and inertial waves that arise in a homogeneous uniformly rotating fluid (Maas 2003), and seem typical for the hyperbolic structure of (3.6). In particular, they signal that the delicate eigenmode structure may give way to the appearance of attractors once some of the symmetric structure in the governing equation, or in the shape and orientation of the fluid domain, is destroyed, as will be discussed later on. Suffice it to say that the solutions obtained are complete and can be used to describe any initial condition (Merzbacher 1970; Gill 1982).

3.1. *Characteristic structure*

With the solution (3.9) of (3.6) in hand it would appear that we would need no further analysis of this case. However, it is useful to emphasize also the underlying characteristic structure. The reason for doing so is that characteristics may provide information about certain properties of the solutions for non-separable cases, that are otherwise difficult to address. We will refer to the collection of a particular characteristic, together with all its boundary reflections, as a characteristic web.

https://doi.org/10.1017/S0022112006002904 Published online by Cambridge University Press

Equation (3.6) has two turning surfaces, at $y_T = \pm\sigma$, where the equation changes from hyperbolic (in the equatorial region) to elliptic (in the polar regions). It can be written as

$$\left(\left(\partial_y - (\sigma^2 - y^2)^{1/2}\partial_z\right)\left(\partial_y + (\sigma^2 - y^2)^{1/2}\partial_z\right) + \frac{y}{(\sigma^2 - y^2)^{1/2}}\partial_z \right)\psi = 0. \tag{3.11}$$

The first term presents the highest-order derivative $\psi_{\eta_+\eta_-}$ in the coordinate frame determined by characteristic coordinates

$$\eta_\pm = z \pm \tilde{y}, \tag{3.12}$$

where

$$\tilde{y} = \tfrac{1}{2}\left[y(\sigma^2 - y^2)^{1/2} + \sigma^2 \sin^{-1}(y/\sigma)\right], \tag{3.13}$$

which are constants of integration of the characteristic equations

$$\frac{\mathrm{d}z}{\mathrm{d}y} = \pm(\sigma^2 - y^2)^{1/2}. \tag{3.14}$$

Observe that two parallel characteristics (labelled 1 and 2) of distance apart $d = \eta_-(1) - \eta_-(2)$, that slant upwards and to the right, do not change distance apart upon reflection from the upper surface (measured by $\eta_+(1) - \eta_+(2) = d$). The same applies also upon reflection at the bottom surface, and again at the turning surfaces, where, as (3.14) shows, the upward and downward slanting characteristics both become horizontal. Figure 1(*a*) gives a picture of the characteristic web in the transformed plane in the case of $m = n = 1$ (i.e. $\pi\sigma_{1,1}^2 = (2m+1)/n = 3$, and with $z' = z$ and $y' = 2\tilde{y}$, $y'_T = \pm(2m+1)/2n = \pm 3/2$, $z'_b = 0$, and $z'_{top} = 1$). In this plane characteristics reflect from the turning surface through a (symmetric) angle.

Characteristics are launched upward and downward at the left turning surface at two different heights. Periodic behaviour of each characteristic web is obvious. However, at the same time the figure is not representative of what happens in cases when bounding surfaces are not symmetric, and the distance between reflecting characteristics changes upon reflection from bounding surfaces. To illustrate this, in figure 1(*b*) we construct a characteristic web for a curved lower boundary. With such a geometry, d changes when characteristics reflect from the bottom. As a consequence, characteristics converge towards a wave attractor (the heavy solid centre lines in figure 1*b*). Note that additional point attractors might arise at the intersections of the turning curves with the lower boundary when $|\, y'_T \,| > |\, y'_G|$, where y'_G denotes the point where the characteristic slope equals the slope of the lower boundary. The examples suggest that separability of the governing equation and simultaneous periodicity (or ergodicity) of each of its characteristic webs are not coincidental, but are two different sides of the same coin.

4. Stern equation

In the second approximation, presented in this section, we focus on Stern's equation (Stern 1963). It keeps non-traditional Coriolis terms but maintains the hydrostatic approximation and considers the fluid to be homogeneous. Historically, this equation can be seen as the starting point for the investigation of equatorial trapping of inertial waves. Although this model was intensively studied in the 1960s and 1970s (Stern 1963; Bretherton 1964; Stewartson 1971, 1972; Israeli 1972) it deserves special attention in our context. The reason is that it can be solved exactly, also for situations with converging characteristics. Therefore, this model is an ideal test case to compare

https://doi.org/10.1017/S0022112006002904 Published online by Cambridge University Press

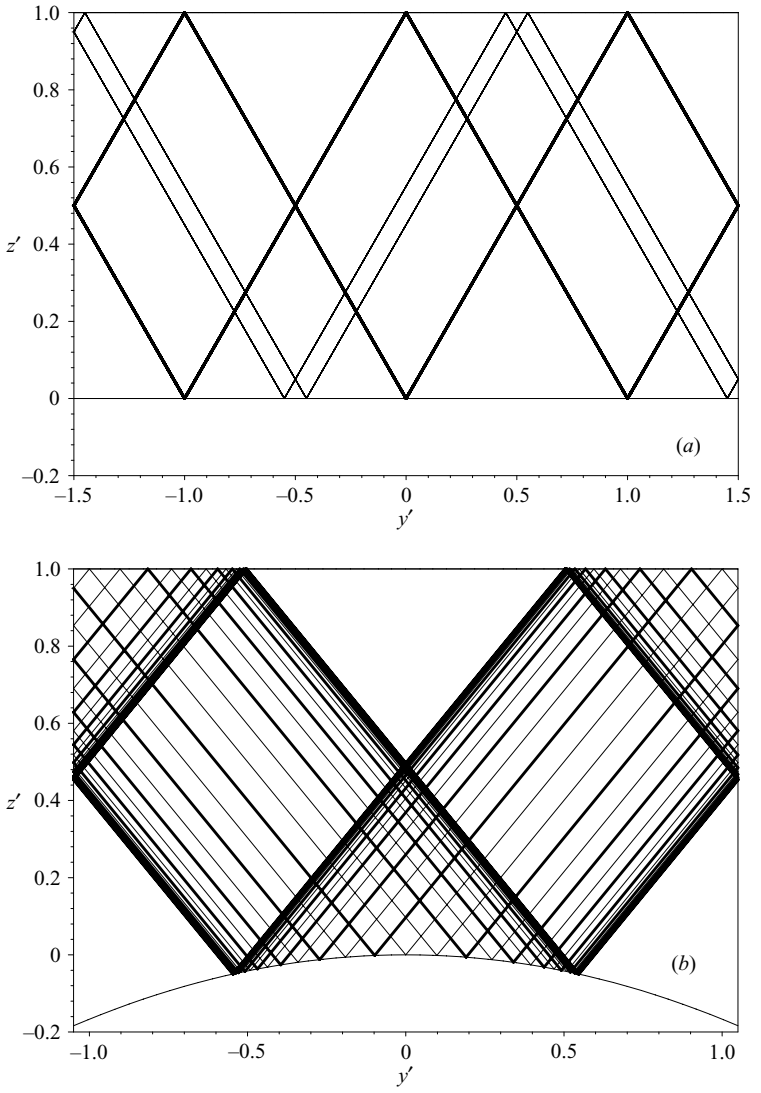


FIGURE 1. Web of characteristics. (*a*) Periodic web for flat geometry and $\pi\sigma^2 = 3$ ($m = 1$, $n = 1$). Two characteristics are launched from the left turning surface $y'_T = -3/2$ at $z' = 0.5$ (thick line) and $z' = 0.95$ (thin line). (*b*) Equatorial wave attractor for $\pi\sigma^2 = 2.1$ ($m = 157$, $n = 150$) when the lower boundary is curved. An upward characteristic (thin line) and a downward characteristic (thick line) are launched from the left turning surface $y'_T = -1.05$ at $z' = 0.95$. The web shows 60 reflections from the boundaries and turning surfaces.

webs of characteristics and solutions. In addition to such comparisons, we discuss some new aspects of Stern's equation, e.g. wave attractors for very low frequencies, overlooked so far in the literature.

Stern (1963) advocated a different scaling of the β-plane equations (2.7)–(2.9). He chose horizontal scale $L = (HR)^{1/2}$, which is of order 160 km and small parameter $\epsilon = (H/R)^{1/2}$, which is about 2.5×10^{-2}. This implies that $\beta = 2\Omega/R = 2\Omega\epsilon/L$. The low-frequency regime is emphasized through the following choice of scales: $[x, z, \sigma, u, w, p] = (L, \epsilon L, 2\Omega\epsilon, U, \epsilon U, 2\Omega HU)$. With this scaling the surface $z = H$

https://doi.org/10.1017/S0022112006002904 Published online by Cambridge University Press

is non-dimensionally equal to $z=1$. Notice that gravity no longer appears in these scalings (the restoring force is solely due to the Coriolis force). This choice of scales leads to non-dimensional equations, in which only the vertical acceleration is preceded by a small parameter $\epsilon^2 = H/R \ll 1$. Neglecting this term, Stern obtains

$$\mathrm{i}\sigma u + w - yv = -p_x, \tag{4.1}$$

$$\mathrm{i}\sigma v + yu = -p_y, \tag{4.2}$$

$$-u = -p_z, \tag{4.3}$$

$$u_x + v_y + w_z = 0. \tag{4.4}$$

and proceeds by considering zonally symmetric waves.† Defining a streamfunction through $v = -\psi_z$ and $w = \psi_y$, the Stern equation follows:

$$\psi_{yy} - (\sigma^2 - y^2)\psi_{zz} + 2y\psi_{yz} + \psi_z = 0. \tag{4.5}$$

The pressure satisfies the same equation. Let us look first for free wave solutions. Using

$$\psi = \phi(y)\sin[n\pi(z - y^2/2)], \tag{4.6}$$

we obtain for ϕ

$$\phi'' + n^2\pi^2\sigma^2\phi = 0. \tag{4.7}$$

For the streamfunction we find, reinserting the exponential time dependence,

$$\psi = \mathrm{Re}\{A_n \exp(\mathrm{i}\sigma[n\pi y + t])\sin[n\pi(z - y^2/2)]\}. \tag{4.8}$$

For a fluid confined between a particular parabolic bottom and surface,

$$z_b = y^2/2, \quad z_s = z_b + 1, \tag{4.9}$$

which in view of the scaling are taken at a unit distance, we have smooth solutions that fulfil the boundary conditions $\psi = 0$ at $z = z_s, z_b$ for any integer n. Owing to the absence of turning (or solid) surfaces in the y-direction no further restrictions are imposed on the frequency σ, so that one obtains a continuous spectrum. As already discussed in § 3.1, the boundary geometry (4.9) is special in the sense that focusing effects are absent and the characteristic web shows either ergodic or periodic behaviour. The problems of finding modal solutions in the case that the bottom and surface are both flat (horizontal) are discussed in a related context by Gerkema & Shrira (2005*a*). However, the important difference between (3.6) and (4.5) is that the latter can also be solved exactly for a geometry where focusing does occur. This opens the possibility for studying the impact of focusing of characteristics on the solutions in physical space.

Let us assume that (4.5) needs to be solved, subject to the conditions that $\psi = 0$ at $z = 0, 1$. This equation is separable, as the differential operator can be split:

$$(\partial_y - (\sigma - y)\partial_z)(\partial_y + (\sigma + y)\partial_z)\psi = 0. \tag{4.10}$$

† Note that upon defining $\tilde{w} = w + p_x$, and inserting (4.3) into (4.4), these equations reduce to the same set that would be obtained when the assumption $\partial_x = 0$ is employed (except that w is replaced by $\tilde{w}$), simplifying the incompressibility relation to $v_y + \tilde{w}_z = 0$. Any zonal structure seems to be absorbable. However, the assumption $p_x = 0$ at $z = 0, 1$ is necessary to obtain the same boundary condition as for the zonally symmetric case, namely $\tilde{w} = 0$ at $z = 0, 1$.

https://doi.org/10.1017/S0022112006002904 Published online by Cambridge University Press

As Stern notes, this equation is satisfied by arbitrary functions $F[(y\pm\sigma)^2/2-z]$. This becomes particularly clear if we introduce a transformation of variables

$$Y = 4y\sigma, \tag{4.11}$$

$$Z = 2(2z - y^2 - \sigma^2), \tag{4.12}$$

that reduces (4.10) to the standard hyperbolic equation

$$\psi_{YY} - \psi_{ZZ} = 0, \tag{4.13}$$

which is thus solved by functions that are constant on straight characteristics $Y \pm Z = c^{\mp}$. Note that the flat bottom and surface ($z = 0, 1$), tangent to the original spherical shell, become two displaced parabola,

$$Z_b(Y) = -2(Y^2/16\sigma^2 + \sigma^2), \quad Z_s(Y) = Z_b(Y) + 4. \tag{4.14}$$

The parabolic shape of (4.14) is the β-plane approximation of the curvature of the underlying spherical surfaces. The fact that in this frame characteristics are straight lines conforms with the intrinsic property of inertial waves in homogeneous rotating fluids that such waves make a fixed angle with the rotation axis, set by the dispersion relation (Greenspan 1968; McEwan 1970; Rieutord, Georgeot & Valdettaro 2001; Maas 2001).

An example of the equatorial wave attractor in the (Y, Z) geometry is shown in figure 2(a). We consider the characteristic web of two characteristics that reflect at the boundaries $z_b, z_s = 0, 1$ and converge towards a wave attractor, similar to the one shown in figure 1(b). (It should be mentioned that characteristics will not end on this attractor for all launching positions. In fact, for some other initial positions, characteristics escape to $Y = \pm\infty$.)

4.1. *Characteristic web method*

The existence of a periodic orbit for a particular frequency was first noted by Bretherton (1964). Stewartson (1971) showed that it was attracting, and argued that the existence of such a wave attractor corresponds to the development of a singularity. However, this argument lacked an explicit construction of the wave field, which will be given here for the first time. It is obtained by using the characteristic web method described in detail by Maas & Lam (1995) and Maas *et al.* (1997). The problem considered here differs from those in Maas & Lam (1995) and Maas *et al.* (1997) in two ways: first, the geometry is concave, and second, the domain of interest is not compact. Nevertheless, the characteristic web method is applicable.

Each point of the fluid domain is reached by exactly two characteristics on which a quantity, called the partial pressure, is constant. The streamfunction and pressure fields at any point are given respectively as the difference and sum of the partial pressures on the two characteristics through that point. Impermeability of the boundaries requires the streamfunction to vanish there, and thus imposes that the partial pressure on each characteristic web is a single unique invariant (Maas 2005). To obtain a well-posed problem, this partial pressure can be set only once on each characteristic web. Thus, it cannot be specified all along the boundary but only in so-called fundamental intervals, $I_n, n \in \{1, 2, 3\}$. In figure 2(a) these fundamental intervals are depicted by thick solid lines at the surface of the equatorial shell and the partial pressure f is specified as $f_{I_i} = \sin\pi((Y - s_{i2})/(s_{i2} - s_{i1}))$, $i = 1, 2$, $f_{I_3} = 1/8$ (from left to right), where s_{i1} and s_{i2} stand for the boundaries of the fundamental intervals. The wave attractor can clearly be seen as a fractal structure showing large streamfunction gradients. More details of

https://doi.org/10.1017/S0022112006002904 Published online by Cambridge University Press

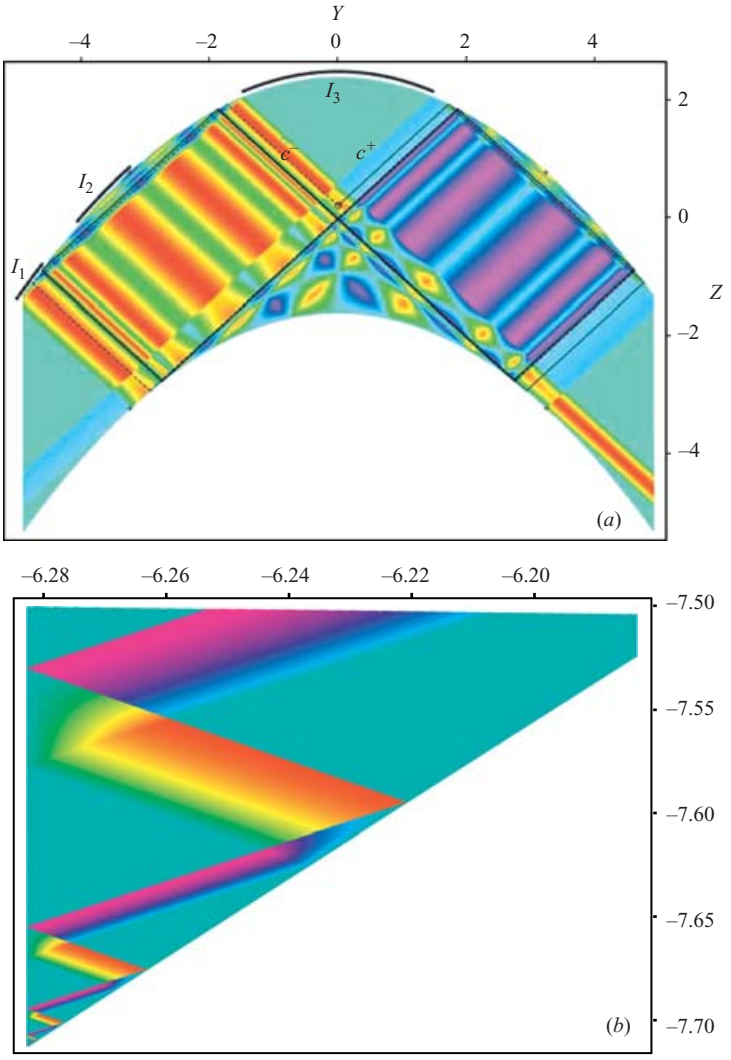


FIGURE 2. Exact streamfunction solutions of Stern's equation for $\sigma = 0.9$. In (a), $f_{I_i} = \sin\pi((Y - s_{i2})/(s_{i2} - s_{i1}))$, $i = 1, 2$, $f_{I_3} = 1/8$. A single web is shown explicitly. A c^+ (solid line) and c^- (dashed line) characteristic is launched at $(Y, Z) = (0, 1/4)$. After four reflections (one reflection) the web of solid lines (dashed lines) intersect with I_1, i.e. both webs converge towards the equatorial wave attractor. The four grazing points are shown by crosses. The three fundamental intervals $I_i, i = 1, 2, 3$ are displayed by thick solid curve segments along the surface. In (b) a lateral boundary is introduced at $Y = -2\pi$. An inertial wave beam is converging towards a point attractor, located at the intersection of the lateral boundary with the bottom.

the wave attractor and also solutions for different frequencies are given by Harlander & Maas (2006*b*).

Interestingly, two 'streamfunction bands' leaving the equatorial wave attractor region can be seen in figure 2(*a*). Owing to the focusing effect at the surface and the bottom, such bands become narrow beams for large $|Y|$. This behaviour can be made visible by placing a wall at $Y_w = \text{const.}$, with $|Y_w| > |Y_G|$, where Y_G-denotes the Y-position of a grazing point. In that case, characteristics cannot reflect back towards

https://doi.org/10.1017/S0022112006002904 Published online by Cambridge University Press

the wave attractor region but become trapped in the region between Y_w and Y_G. Figure 2(*b*) shows the area close to the intersection of a lateral boundary (placed at $Y_w = -2\pi$) with the bottom. One can see a beam reflecting endlessly between the lateral and the lower boundary. The self-similar structure of the beam is obvious. A point attractor is located at the intersection of the two boundaries. In § 5, a behaviour similar to this is found at intersections between bottom and turning surfaces. Turning surfaces come into play by introducing stratification.

4.2. *Attractor diagram*

Israeli (1972) observed that Stern's (1963) frequencies were the upper limit of continuous frequency ranges for which such attractors can be found. Frequencies of wave attractors are thus not discrete, but belong to an infinite set of compact (frequency) intervals. This result can be appreciated by simply tracing characteristics, launched at the surface at some latitude y_0, in either the northward ($\sigma > 0$) or southward ($\sigma < 0$) direction and observing whether the characteristic, as a function of frequency and launching latitude, shoots off to positive (red) or negative infinity (yellow) ('north' or 'south pole'), or stays in the vicinity of the equator, see figure 3(*a*). This figure shows the infinite set of attractor frequency bands (blue). For the biggest windows these correspond to the bounding frequencies given by Stewartson (1972), e.g. the frequency interval $[0.8165\ldots, 0.9428\ldots]$. By inspecting figure 3(*a*, *b*) we note that besides the set of 'high'-frequency windows of equatorial wave attractors (Stewartson & Rickard 1969; Stewartson 1971, 1972; Israeli 1972) there also exists a set of low-frequency windows (frequencies less than 0.5) which appears to have been overlooked so far. Note that in contrast to figure 3(*a*), attractor frequency bands are shown as black areas in (*b*), and the rate of divergence to $\pm\infty$ is indicated by the grey scale. The lowest attractor frequency ($\sigma = 0.5$) found by Stern (1963) corresponds to an attractor with a single cell (three reflections at the surface and one at the bottom), whereas the attractor frequencies $\sigma > 0.9$ tabulated by Stewartson (1971) correspond to attractors with an even number of cells $2\ldots10$, lined up in the y-direction (see figure 3*c*). Attractors with frequencies lower than $\sigma = 0.5$ have typically more than one cell in the y- and z-direction. For example the attractor with frequency $\sigma = 0.37$ (which is the frequency band next to $\sigma = 0.5$) has six cells in total, corresponding with eight points of surface reflections (figure 3*c*). In this case three of the cells are lined up vertically on each side of the $Y = 0$ axis (Harlander & Maas 2006*b*). Note that within a certain frequency band the wave attractor can change its appearance. For example by choosing a frequency of $\sigma = 0.52$, the single cell attractor found for $\sigma = 0.5$ breaks up into two independent one-cell attractors, located asymmetrically with respect to the $Y = 0$ axis. Such an asymmetry is obvious in figure 3(*c*) which shows one of the two asymmetrically situated attractors. This means that for $\sigma = 0.52$ (including the attractors at $\pm\infty$) we have four co-existing attractors in total.

Stewartson (1971) and Stewartson & Walton (1976), expressing bewilderment at the singular nature of the focusing inertial waves, managed to find convergence rates and even a viscous description of the focused state. Recent work on thick spherical shells (motivated by astrophysical problems) confirms the importance of these findings (Tilgner 1999; Rieutord *et al.* 2001; Ogilvie & Lin 2004).

5. Stratified Stern equation

In a third approximation to the governing equations (2.7)–(2.9), we here extend Stern's equation to include uniform stratification, more appropriate for geophysical

https://doi.org/10.1017/S0022112006002904 Published online by Cambridge University Press

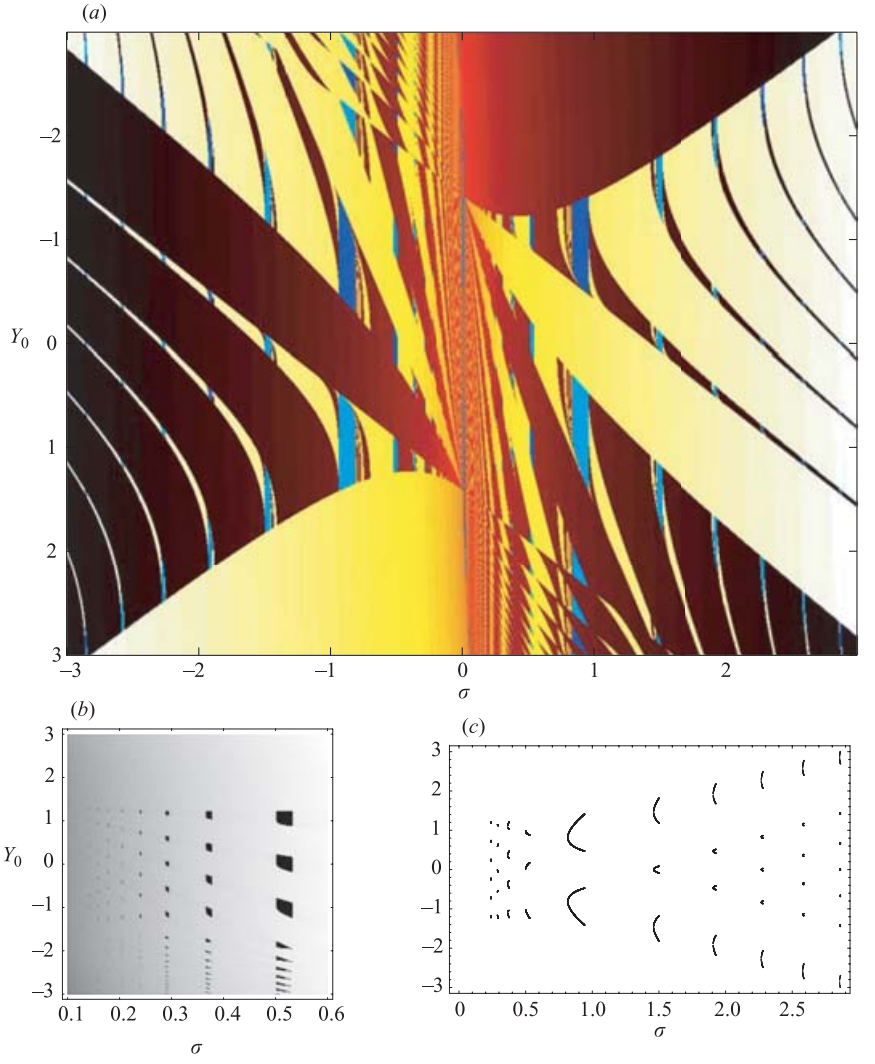


FIGURE 3. Attractor diagrams. In (*a*) the blue areas indicate the existence of an equatorial wave attractor. The red (yellow) scale indicates the rate of divergence of the characteristics to $+\infty$ ($-\infty$). The frequency intervals tabulated by Stewartson (1972) ([0.8165, 0.9428], [1.4606, 1.5005], [1.9072, 1.9274], [2.2680, 2.2807], [2.5787, 2.5877]) correspond to some of attractor frequency intervals shown. In (*b*) a blow-up of the low-frequency region ($0.1 < \sigma < 0.6$) is shown. Black areas correspond to attractors, and for $Y_0 < -1.5$ to domains of attraction. The grey scale indicates rate of divergence to $\pm\infty$. In (*c*) points are shown where the attractors touch on the surface for frequencies in the range $1/5 < \sigma < 3$.

applications. Owing to the stratification, characteristics are trapped near the equator by turning surfaces, a feature which is present for the standard model and for the classical equatorially trapped wave solutions too, but which is absent for the original (unstratified) Stern equation. In addition to the equatorial wave attractors, point attractors also appear, at the intersections of turning surfaces and the bottom. For thin shells, these turning surfaces are located very close to the inertial latitudes corresponding to the wave's frequency. Here, these waves are perceived as (near) inertial oscillations. These inertial wave attractors are manifested as traps for

https://doi.org/10.1017/S0022112006002904 Published online by Cambridge University Press

downward-propagating inertia–gravity waves. Therefore, a remarkable consequence of the introduction of stratification is that, in contrast to Stern's original equation, waves of all frequencies are trapped, either on an equatorial wave attractor or on an inertial wave attractor at the bottom.

We now choose scales $[x, z, \sigma, u, w, p, b, N] = (R, R, 2\Omega, U, U, 2\Omega UR, 2\Omega U, 2\Omega)$. Recall that $\beta = 2\Omega/R$. Again we consider zonally symmetric ($\partial_x = 0$) waves only, which leads to the following equations:

$$\mathrm{i}\sigma u + w - yv = 0, \tag{5.1}$$

$$\mathrm{i}\sigma v + yu = -p_y, \tag{5.2}$$

$$\mathrm{i}\sigma w - u = -p_z + b, \tag{5.3}$$

$$\mathrm{i}\sigma b + wN^2 = 0, \tag{5.4}$$

$$v_y + w_z = 0. \tag{5.5}$$

It should be noticed that in these equations no terms are discarded as yet, in contrast to the two previous derivations, for strongly stratified and unstratified thin shells respectively. Note that with this scaling the fluid domain is now confined to a depth $\epsilon^2 = H/R \ll 1$, and one considers waves whose vertical and horizontal velocities may be of the same order of magnitude. This merely serves as an intermediate scaling that will be discarded below, but which is helpful in obtaining the following equation for the streamfunction:

$$\Gamma\psi_{yy} - (\sigma^2 - y^2)\psi_{zz} + 2y\psi_{yz} + \psi_z = 0, \tag{5.6}$$

where

$$\Gamma = 1 + N^2 - \sigma^2. \tag{5.7}$$

This equation is a simplified version of the Eliassen–Sawyer equation (Hua, Moore & Gentil 1997) (for time-harmonic waves)

$$-\sigma^2\nabla^2\psi + \frac{\partial}{\partial z}\left(A\frac{\partial\psi}{\partial z} + B\frac{\partial\psi}{\partial y}\right) + \frac{\partial}{\partial y}\left(B\frac{\partial\psi}{\partial z} + C\frac{\partial\psi}{\partial y}\right) = 0, \tag{5.8}$$

where $A = \beta y(\beta y - U_y)$, $B = \beta y(2\Omega + U_z)$, $C = N^2 + 2\Omega(2\Omega + U_z)$, in which shear in the zonal background flow U is neglected and in which the above scaling is applied. Under these conditions the coefficients are $A = y^2$, $B = y$, and $C = N^2 + 1$. Following Ooyama (1966), a necessary condition for instability is that $B^2 - AC \geqslant 0$. Since here $B^2 - AC = -N^2y^2$, our model (5.6) is stable in the classical sense. Nevertheless, instability can be expected due to the presence of wave attractors. We will come back to this point in § 6.

With a rescaled meridional coordinate

$$y' = y/\Gamma^{1/2} \tag{5.9}$$

we obtain what shall be referred to as the stratified Stern equation:

$$\psi_{y'y'} - (\sigma^2 - \Gamma y'^2)\psi_{zz} + 2y'\psi_{y'z} + \psi_z = 0. \tag{5.10}$$

This reduces to the separable Stern equation (4.5) for $\Gamma = 1$ (for which $y' = y$). Surprisingly, this corresponds to buoyancy waves (for which $\sigma = N$, see (5.7)), rather than to waves of arbitrary (low) frequency in a non-stratified medium. Indeed, neglect of the vertical acceleration (last term in the equation for Γ, (5.7)), together with a vanishing stratification ($N = 0$), superficially leads to the same limit. Note that

https://doi.org/10.1017/S0022112006002904 Published online by Cambridge University Press

in certain shear flows such buoyancy waves can even be solutions of the Eliassen–Sawyer equation. This equation transforms to (4.5) when a zonal basic flow of the form $\bar{U} = u_0 + u_1(z - y^2/2)$ is assumed (u_0 and u_1 constants) and waves with frequency $\sigma(1+u_1)^{-1/2}$ are considered. Notice further, how, with the neglect of the last two terms of (5.10), and the first and last terms in the expression for Γ, (5.7), we recover (3.6). This equation was obtained in the traditional approximation, that yields the Weber equation, suggesting discretized modes for flat upper and lower boundaries.

For the particular parabolic bottom and surface, in which we take account of the scaling by assuming them to be $\epsilon^2 = H/R$ apart,

$$z_b = y'^2/2, \quad z_s = z_b + \epsilon^2, \tag{5.11}$$

we can again find discretized modes of smooth solutions of (5.10) that vanish at the curved top and bottom, as well as at $y' \to \pm\infty$. In terms of Hermite polynomials $H_m(\eta)$ these are

$$\psi_{mn} = H_m(\eta)\,\mathrm{e}^{-\eta^2/2}\sin[n\pi\epsilon^{-2}(z - y'^2/2)], \tag{5.12}$$

where

$$\eta = y'\sigma_{mn}n\pi/(2m+1)^{1/2}\epsilon^{-2}. \tag{5.13}$$

Quantized eigenfrequencies σ_{mn} are solutions of the quartic

$$\omega_{mn}^{-2}\sigma^4 + \sigma^2 - N^2 = 0, \tag{5.14}$$

defined in terms of frequencies

$$\omega_{mn} = \frac{2m+1}{n\pi}\epsilon^2. \tag{5.15}$$

For low frequencies, $\omega_{mn} \ll N$, the eigenfrequencies are given approximately by

$$\sigma_{mn} \approx \pm(\omega_{mn}N)^{1/2}, \tag{5.16}$$

which reduces to (3.10), the spectrum of the standard equation, provided differences in scaling are taken into account.

In contrast to the non-stratified situation, the solutions show turning latitudes, i.e. they are exponentially damped beyond a certain distance y'_T. As already mentioned in §§3.1 and 4, the particular parabolic choice of boundaries (5.11) is unusual in the sense that focusing effects are absent and the characteristic web shows periodic behaviour.

To obtain information on solutions for general geometry, let us now turn to the characteristics of (5.10). With

$$D(y') = \sigma(1 - \Lambda^2 y'^2)^{1/2} \tag{5.17}$$

and $\Lambda = ((N/\sigma)^2 - 1)^{1/2}$, equation (5.10) transforms into

$$(\partial_{y'} + (y' - D)\partial_z)(\partial_{y'} + (y' + D)\partial_z)\psi + D_{y'}\psi_z = 0. \tag{5.18}$$

Characteristics of (5.18) are determined as solutions of (John 1975)

$$\frac{\mathrm{d}z}{\mathrm{d}y'} = y' \pm \sigma(1 - \Lambda^2 y'^2)^{1/2}. \tag{5.19}$$

Owing to the last, single-derivative term, (5.18) is not separable and thus not solvable. Nevertheless, for short waves, the characteristics of (5.18) correspond to energy paths (Harlander & Maas 2006*a*) and therefore they contain valuable information on

https://doi.org/10.1017/S0022112006002904 Published online by Cambridge University Press

solutions of (5.18). These characteristics are real, provided the meridional extent y' is restricted to be between two turning distances $\pm y'_T$, where

$$y'_T \equiv 1/\Lambda. \tag{5.20}$$

For $\sigma \ll N$ this is at $y'_T \approx \sigma/N$, or, in terms of y, at $y_T \approx R\Gamma^{1/2}\sigma/N$, dimensionally equal to $R\sigma/2\Omega$. This turning distance corresponds, via $y = R\phi$, to a turning latitude $\phi = \sigma/2\Omega$. However, for small latitudes $\phi \approx \sin\phi = f/2\Omega$, with f the local inertial frequency. Therefore, the turning latitude is located very close to the wave's inertial latitude, where the wave returns equatorwards, so that, from a local perspective, its frequency becomes superinertial again. For this reason, we will refer to the turning latitude loosely as the inertial latitude. The turning distance (5.20) is itself real for waves of frequency less than or equal to the buoyancy frequency.

5.1. *Turning surfaces*

With the addition of stratification the existence of turning surfaces was discussed on the classical β-plane in the context of the harmonic oscillator equation, there giving rise to Airy solutions (Munk & Phillips 1968; Stewartson & Walton 1976; Munk 1980; Fu 1981). In that context, the (trivial) vertical dependence is split off and the turning surfaces reduce to turning points occurring only in the meridional direction. Considering inertia–gravity waves, Friedlander & Siegmann (1982) discovered that in the full sphere axially symmetric turning surfaces arise whose position depends on the radial coordinate. For the geophysically relevant regime $N > 2\Omega$, these surfaces are hyperboloids of revolution. When supplied with a spherical inner boundary, the fluid domain thus bounded by surface, bottom and sloping turning surfaces, again leads to focusing of characteristics (Dintrans, Rieutord & Valdettaro 1999). The present analysis in fact puts a microscope on this model configuration for the oceanographically (and meteorologically) relevant case of a thin equatorial shell. With this restriction we aim to achieve a description which is both relatively simple, and yet recovers the important and relevant features, such as turning surfaces and grazing characteristics.

5.2. *Web of characteristics*

The characteristic equations (5.19) suggest a transformation

$$\eta = \Lambda y', \tag{5.21}$$

$$\zeta = \Lambda^2 z, \tag{5.22}$$

and parameter

$$s = \sigma\Lambda = (N^2 - \sigma^2)^{1/2}, \tag{5.23}$$

so that $|\eta| \leqslant 1$, and the turning surfaces (inertial latitudes), in this scaling, appear fixed at $\eta_T = \pm 1$. Note that this transformation implies that the surface is now found at

$$h \equiv \Lambda^2 \frac{H}{R} = \left(\frac{N^2}{\sigma^2} - 1\right)\frac{H}{R}, \tag{5.24}$$

which approaches 1 (for frequency $\sigma \ll N$) at $\sigma = \epsilon N$. Note that from (5.7) $\Gamma = 1 + s^2$. The solutions of the characteristic equations (5.19) are then given by

$$\zeta_\pm = \frac{1}{2}\eta^2 \pm c \pm \frac{s}{2}\left(\eta(1-\eta^2)^{1/2} + \sin^{-1}\eta\right), \tag{5.25}$$

where c is an undetermined constant of integration. There are thus two families of characteristics, referred to as positive or negative according to the sign in (5.25).

https://doi.org/10.1017/S0022112006002904 Published online by Cambridge University Press

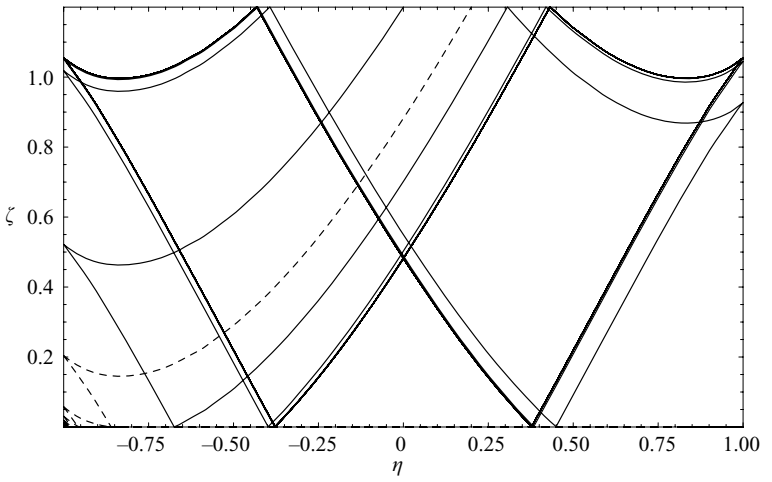


FIGURE 4. Webs of characteristics in a non-traditional uniformly stratified equatorial β-plane, showing simultaneous approach of an equatorial wave attractor (solid line), and an inertial point attractor (lower bottom left corner, dashed line) for rays starting at different meridional surface positions. Here $h = 1.2$, $s = 1.5$, i.e. according to figure 6, the attractors belong to the regime 'one surface intersection.'

Each characteristic of one family is vertically displaced from any other member of that family. The two families are of mirror images each other, when reflected in the equator.

To identify wave attractors we construct an algorithm that ties the characteristics of the two families together at the points of reflection, i.e. at intersections of the characteristics with the surface and bottom boundary and with the two lateral turning surfaces. By using such an algorithm (the Appendix), we find that two to four co-existing attractors typically occur. Each of them has its own domain of attraction. Two of these attractors are point attractors, situated in the bottom corners at $(\pm 1, 0)$. These have a permanent character in that they exist for every $\sigma < N$. The other single attractor or two attractors consist of a symmetric or a mirror-pair of asymmetric, equatorial wave attractors, respectively. In figure 4 there are three co-existing attractors, two of which are shown by means of their web of characteristics. Starting at $(\eta, \zeta) = (0, h)$, with $h = 1.2$, the characteristics converge towards an equatorial wave attractor (solid line). This attractor resembles the one in the example shown for the standard equation with bottom topography (cf. figure 1*b*), as well as the one discussed for Stern's equation (cf. figure 2*a*). In contrast, a characteristic launched at $(0.2, 1.2)$ is attracted by the inertial wave attractor at the lower left corner (dashed line), whereas the lower right corner would attract a characteristic launched at $(-0.2, 1.2)$. Note that such point attractors exist neither for the Stern equation without lateral boundaries, nor for the standard equation with a flat bottom. However, as mentioned before, such point attractors are possible for the standard equation if the bottom topography has a supercritical slope at the turning surfaces. Of course, as shown in figure 2(*b*), point attractors also exist for the Stern model if lateral boundaries are introduced beyond the grazing points.

In view of the fact that the turning surface is situated almost at the inertial latitude, the waves that turn to the point attractors are perceived there as inertial oscillations. Given the fact that in attractor diagrams (for given stratification and rotation rate) we find these point attractors to occur generically, for every given frequency, we conclude

https://doi.org/10.1017/S0022112006002904 Published online by Cambridge University Press

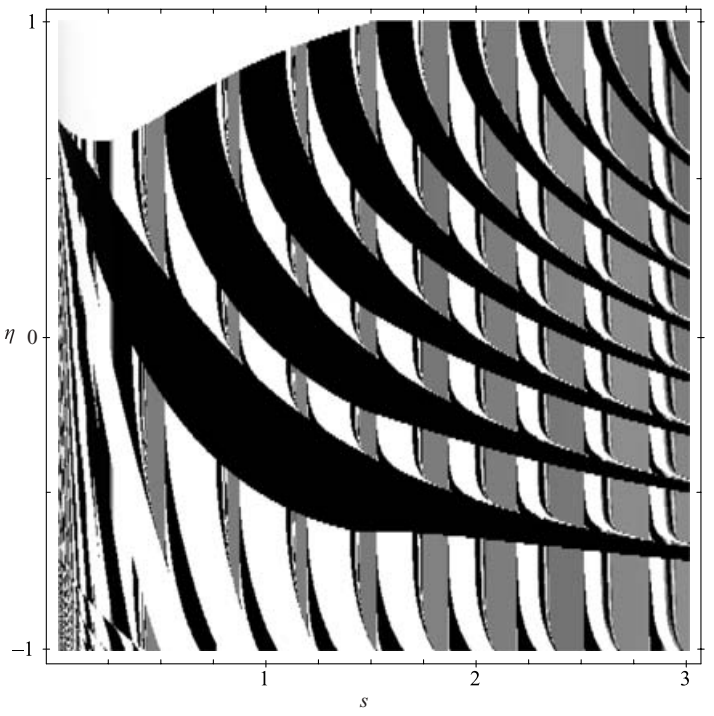


FIGURE 5. Attractor diagram for a stratified non-traditional equatorial β-plane. The (one-sided) diagram, shows the occurrence of equatorial wave attractors (grey), co-existing with inertial latitude point attractors (black $\eta = 1$, white $\eta = -1$), reached from launching position η_0, being launched upon the positive characteristic at the surface for given value of s. For fixed ratio of buoyancy and wave frequency (i.e. fixed h and aspect ratio H/R), the frequency of the wave is directly proportional to that parameter $\sigma = s(H/Rh)^{1/2}$. Here $h = 1/4$, so that in the ocean $\sigma \approx s/20$, for $s = 1$ dimensionally corresponding to a period of 10 days.

that inertial oscillations attract a substantial part of the waves generated within the corresponding wave domain.

Figure 3 showed an attractor diagram for Stern's equation. From this diagram one can read off the frequency bands for which equatorial wave attractors exist. The corresponding diagram for the stratified Stern equation is shown for positive frequencies in figure 5. Positive characteristics are launched at the surface between the turning surfaces (in the interval $[-1, 1]$) for different values of $s = \sigma(H/Rh)^{-1/2}$. The black areas indicate trapping of characteristics at the lower right, that is the northern point attractor of figure 4; and correspondingly for the white areas. The grey regions show frequency bands where equatorial wave attractors exist. Note that the abscissa corresponds to that of figure 3 when multiplied by 1/2. (For Stern's equation we scaled σ by $2\Omega(H/R)^{1/2}$ whereas s is scaled by $2\Omega(H/Rh)^{1/2}$, where $h = 1/4$.) Qualitatively, figure 3 and figure 5 are similar. The most striking difference is the increase of the width of the equatorial wave attractor frequency bands with increasing frequency. It appears that for the stratified Stern equation, more energy is trapped at equatorial wave attractors. Note further that a significant part of the energy might be radiated away from the equatorial region when $N = 0$. In contrast, if stratification is larger than 2Ω, all waves are trapped between the turning surfaces.

https://doi.org/10.1017/S0022112006002904 Published online by Cambridge University Press

6. Discussion

The present paper has looked at a highly idealized geophysical situation: monochromatic, zonally symmetric, linear waves in an equatorial band of a spherical shell that is filled with either a homogeneous or a uniformly stratified inviscid fluid. In some cases explicit solutions were obtained; in others, conclusions were based on the behaviour of characteristics of the governing equation, arguing that they also represent energy propagation paths (Harlander & Maas 2006*a*). The conclusions drawn here, however, are relevant. They suggest that classical models of equatorial waves are all too symmetrized. Thus they lack the typical focusing property that is responsible for the piling up of wave energy around a wave attractor, and that should be discernible in viscous models too. Indeed, wave attractors were found numerically in viscous models in the spherical shell (Rieutord & Valdettaro 1997; Dintrans *et al.* 1999; Rieutord, Georgeot & Valdettaro 2000, 2001; Rieutord, Valdettaro & Georgeot 2002; Tilgner 1999) and tilted square (Ogilvie 2005), and were moreover observed experimentally in trapezoidal containers (Maas 2001; Manders & Maas 2003, 2004). This shows that a localized increase of energy density and the establishment of a wave attractor does not in practice need an infinite number of reflections from 'perfect' boundaries. Clearly, the number of reflections, the final actual width of the attractor, as well as the time needed for its establishment will be limited by viscous and nonlinear processes that were not addressed in this paper. This is an interesting issue for future studies.

But, is there any evidence for the existence on a geophysical scale of the two types of attractors encountered here, the inertial and equatorial wave attractors? At first sight, the requirements for finding exact (viscous) analogues of wave attractors in the field seem formidable. Particularly in the oceans, the presence of continents seems to prohibit the use of zonally symmetric waves. But waves, having a zonal propagation component, are subject to focusing reflections from the surface or turning surface and refract instantaneously towards the meridional plane at each such reflection as described for inertial (Manders & Maas 2004) and internal gravity waves (Maas 2005). As a consequence, the waves may become trapped in that plane. As this occurs at each zonal section, the wave field might obtain a zonally uniform character.

Inertial wave attractors appear where turning surfaces intersect the bottom. At this intersection, the wave frequency is very close to the local inertial frequency. Therefore this picture suggests that in the deep ocean, close to the inertial latitude (where the downward-propagating inertia–gravity waves are trapped), inertial oscillations should be intensified (Maas 2001). Recently, Gerkema & Shrira (2005*b*) discussed the occurrence of deep-ocean point attractors in a model similar to the stratified Stern equation but tuned for the extratropics. For midlatitudes they estimate the portion of bottom-trapped internal wave energy to be roughly 10 %–30 %. Such a prominent vertical asymmetry in the distribution of near-inertial wave energy should be detectable by deep-ocean soundings. Indeed, van Haren, Maas & van Aken (2002) and van Aken, Maas & van Haren (2005) reported the finding of persistent, abyssally intensified inertial motions near a continental slope. More evidence comes from yearlong records of near-equator deep-water data (van Haren 2005). Spectra of near-inertial motions obtained from these data show enhanced power in a narrow latitude band around the equator ($\phi \in [-2^\circ, 2^\circ]$). Moreover, in this band the stability profile possesses more 'steppiness', which is an indication of enhanced mixing. Oceanic equatorial wave attractors might be related to observed, remarkably stable and zonally uniform deep equatorial jets, and to observed elongated zonal patterns in scatterometer data. An important aspect of wave focusing and wave attractors is

https://doi.org/10.1017/S0022112006002904 Published online by Cambridge University Press

mean flow generation by fluid mixing. Evidence of this comes e.g. from dye spreading in inertial wave experiments, see Maas (2001). Mixing due to wave attractors might be an alternative to more established mixing concepts (like classical mean flow instability or convection), explaining onset and existence of equatorial jets both in oceans as well as on giant planets (Galperin *et al.* 2004; Ogilvie & Lin 2004). Driving by inertia–gravity waves in the meridional plane might in principle operate at a significant distance away from the surface where obvious momentum sources are found (wind and buoyancy forcing). The suggestion from our study is that geometric focusing of inertia–gravity waves intensifies motion and shear to the point of wave breaking. In particular, intensification is expected near the focusing surface reflections of equatorial wave attractors and near the bottom at the inertial wave attractors.

Recent scatterometer data (Gille, Smith & Statom 2005), obtained from satellite observations, might also contain a footprint of the meridional propagation of internal waves, and perhaps even of their localization. Scatterometer data are conventionally seen as providing wind speed information (through the surface gravity waves that are generated), and Gille *et al.* (2005) interpret their data in such terms, with particular emphasis on the diurnal land-breeze wind system encountered close to the coast. However, equatorward of 30°, diurnal signals were found to be present over the whole Pacific and Atlantic oceans, stretching out as elongated bands parallel to the equator, which they attribute to local convective winds. But, surface gravity waves may also be modulated by straining motions associated with subsurface internal gravity waves. In this interpretation, the coherent, elongated zonal structures observed by the scatterometer might in fact point to the presence of locally amplified, focused diurnal internal tides.

Previously, instabilities in formally stable conditions appeared as perturbations of a stratified flow in the presence of a mean shear (Farrell 1982; Hua *et al.* 1997; Yavneh, McWilliams & Molemaker 2001). Here, however, we find that a localized instability does not need a shear flow at all, but appears in virtually all confined stably stratified fluids (whether non-rotating and stratified, non-stratified and uniformly rotating, or a combination of both). This instability is induced essentially by an initially random noise field of obliquely propagating inertia–gravity waves. Provided the fluid sustains sufficient boundary reflections (against the ever-present damping or wave–wave interaction processes) the focusing of these waves at these reflections may amplify gradients to the extent that they locally trigger one of the classical instabilities. Thus, while intimately related to one of these classical instabilities, each case is encompassed in the term 'geometric instability' and is induced essentially by the single-angled nature of wave propagation in a container having a symmetry-breaking geometry.

We thank Frans Eijgenraam for computational support. U. H. is supported by a grant from the Dutch National Science foundation NWO. We acknowledge constructive suggestions and helpful comments on lucid writing by an anonymous referee.

Appendix. Iteration algorithm to find webs of characteristics for the stratified Stern equation

A characteristic curve of the negative family of characteristics reaches its minimum height at

$$\eta_c = s/(1+s^2)^{1/2}. \tag{A 1}$$

https://doi.org/10.1017/S0022112006002904 Published online by Cambridge University Press

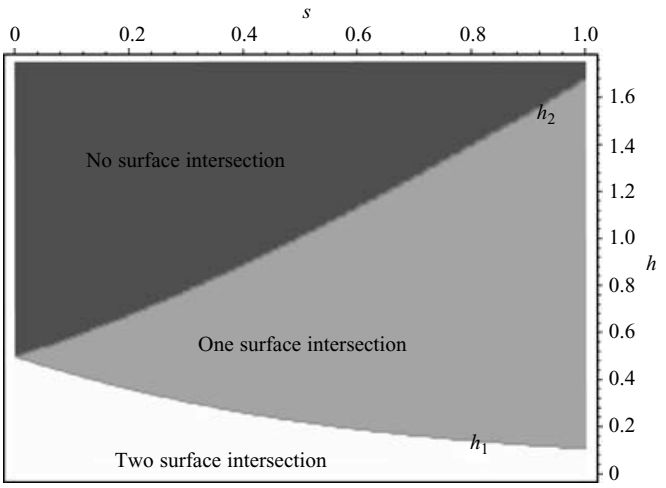


FIGURE 6. Phase plane (s, h) division. The two lines $h_{1,2}$ separate regions for which grazing characteristics have 0, 1 or 2 intersections with the surface at $\zeta = h$, for $|\eta| \leqslant \eta_T = 1$.

Members of the positive family have a minimum at $-\eta_c$. An important role is played by the so-called grazing characteristics (thick lines) for which a particular characteristic curve's minimum is at the bottom. This is found at

$$c_g = -\eta_c^2/2 + s\left(\eta_c\left(1-\eta_c^2\right)^{1/2} + \sin^{-1}\eta_c\right)/2 = s\sin^{-1}(\eta_c)/2 = s\tan^{-1}(s)/2, \qquad (A\,2)$$

where we have used (A 1). The grazing characteristic singularity was first discussed in Stewartson & Rickard (1969), see also discussion in Rieutord *et al.* (2000). The maximum value of the constant c is for the negative family of curves, reached at η_c at the surface $\zeta = h$. We thus find

$$c_{max} = h + c_g. \qquad (A\,3)$$

Similarly, the minimum value of the negative family of curves is found in the bottom corner at $(\eta, \zeta) = (-1, 0)$, and is

$$c_{min} = -1/2 - s\pi/4. \qquad (A\,4)$$

At turning surfaces ($\eta = \pm 1$) reflecting characteristics have the same slope. Three regimes can be distinguished, depending on the number of intersections of the grazing characteristic with the surface. For $0 < h \leqslant h_1$ it has two surface intersections, for $h_1 < h \leqslant h_2$ one, and for $h_2 < h$ it has no surface intersections. The bounding 'heights' $h_{1,2}$ are found when the grazing characteristic (of the negative family) goes through the surface corner at $\eta = +1$ and $\eta = -1$, respectively. The negative characteristics through these corners $(1, h)$ and $(-1, h)$ have constant $c_+ = h - 1/2 + s\pi/4$ and $c_- = h - 1/2 - s\pi/4$, respectively. Identifying these constants with c_g leads to

$$h_1 = \tfrac{1}{2}\left(1 - s\sin^{-1}\left(1/(1+s^2)^{1/2}\right)\right) = \tfrac{1}{2}(1 - s\cot^{-1}s) \qquad (A\,5)$$

and

$$h_2 = \tfrac{1}{2}(1 + s(\pi - \cot^{-1}s)). \qquad (A\,6)$$

This divides the (s, h)-plane into three regions, where different iteration algorithms apply, telling us whether subsequent reflections are from the side or top wall (see figure 6). Subsequently, we aim to identify webs of characteristics, consisting of

https://doi.org/10.1017/S0022112006002904 Published online by Cambridge University Press

sets of characteristic curve segments that belong successively to the positive and negative family (or vice versa, depending on the initial family) and that share a reflection point at the bottom, surface or one of the turning surfaces. Therefore, the algorithm that ties the characteristics together requires finding intersections of characteristics with each of the four boundaries. Reflection at the turning surfaces is easy. Take for instance that at $\eta = 1$. Let the constant of the incoming negative characteristic be denoted c_n. Here n is an integer signifying the nth segment resulting upon launching at η_0 with sign + or −. This characteristic will reflect from the turning surface at a height $\zeta_n = 1/2 + c_n - s\pi/4$. The constant labelling the reflecting, positive characteristic, c_{n+1}, is then determined simply from $\zeta_n = 1/2 + c_{n+1} + s\pi/4$, so that $c_{n+1} = c_n - s\pi/2$. Reflection at the surface and bottom, however, requires the solution of a transcendental equation, which seems analytically intractable, and has for this reason been solved using a standard Newton–Raphson root-finding algorithm. With it we determine reflection point η_n, and, from that, deduce the constant c_{n+1}, labeling the reflecting characteristic.

REFERENCES

van Aken, H. M., Maas, L. R. M. & van Haren, H. 2005 Observations of inertial wave events near the continental slope off Goban Spur. *J. Phys. Oceanogr.* **35**, 1329–1340.

Bretherton, F. P. 1964 Low frequency oscillations trapped near the equator. *Tellus* **16**, 181–185.

Dintrans, B., Rieutord, M. & Valdettaro, L. 1999 Gravito-inertial waves in a rotating stratified sphere or spherical shell. *J. Fluid Mech.* **398**, 271–297.

Farrell, B. 1982 The initial growth of disturbances in a baroclinic flow. *J. Atmos. Sci.* **39**, 1663–1686.

Friedlander, S. & Siegmann, W. L. 1982 Internal waves in a rotating stratified fluid in an arbitrary gravitational field. *Geophys. Astrophys. Fluid Dyn.* **19**, 267–291.

Fu, L. L. 1981 Observations and models of inertial waves in the deep ocean. *Rev. Geophys. Space Phys.* **19**, 141–170.

Galperin, B., Nakano, H., Huang, H.-P. & Sukoriansky, S. 2004 The ubiquitous zonal jets in the atmospheres of giant planets and Earth's oceans. *Geophys. Res. Lett.* **31**, L13303, doi:10.1029/2004GL019691.

Gerkema, T. & Shrira, V. I. 2005*a* Near-inertial waves in the ocean: beyond the 'traditional approximation'. *J. Fluid Mech.* **529**, 195–219.

Gerkema, T. & Shrira, V. I. 2005*b* Near-inertial waves on the 'non-traditional' β plane. *J. Geophys. Res.* **110**, C01003, doi:10.1029/2004JC002519.

Gill, A. E. 1982 *Atmosphere-Ocean Dynamics*. Academic.

Gille, S. T., Smith, S. G. L. & Statom, N. M. 2005 Global observations of the land breeze. *Geophys. Res. Lett.* **32**, L05605, doi:10.1029/2004GL022139.

Greenspan, H. 1968 *The Theory of Rotating Fluids*. Cambridge University Press.

van Haren, H. 2005 Sharp near-equatorial transitions in inertial motions and deep-ocean step-formation. *Geophys. Res. Lett.* **32**, L01605, doi:10.1029/2004GL021630.

van Haren, H., Maas, L. R. M. & van Aken, H. 2002 On the nature of internal wave spectra near a continental slope. *Geophys. Res. Lett.* **29**(12), doi:10.1029/2001GL014341.

Harlander, U. & Maas, L. R. M. 2006*a* Characteristics and energy rays of equatorially trapped, zonally symmetric internal waves. *Met. Z.* **15**, 439–450.

Harlander, U. & Maas, L. R. M. 2006*b* On inertial boundary layers in a well mixed equatorial atmosphere. *Dyn. Atmos. Oceans* (submitted).

Høiland, E. 1962 Discussion of a hyperbolic equation relating to inertia and gravitational fluid oscillations. *Geophys. Publ.* **XXIV**, 211–227.

Hua, B. L., Moore, D. W. & Gentil, S. L. 1997 Inertial nonlinear equilibration of equatorial flows. *J. Fluid Mech.* **331**, 345–371.

Israeli, M. 1972 On trapped oscillations of rotating fluids in spherical shells. *Stud. Appl. Maths* **L1**, 219–237.

John, F. 1975 *Partial Differential Equations*, 2nd edn. Springer.

https://doi.org/10.1017/S0022112006002904 Published online by Cambridge University Press

Maas, L. R. M. 2001 Wave focusing and ensuing mean flow due to symmetry breaking in rotating fluids. *J. Fluid Mech.* **437**, 13–28.

Maas, L. R. M. 2003 On the amphidromic structure of inertial waves in a rectangular parallelepiped. *Fluid Dyn. Res.* **33**, 373–401.

Maas, L. R. M. 2005 Wave attractors: linear yet nonlinear. *Intl J. Bifurcation Chaos* **15**, 2757–2782.

Maas, L. R. M., Benielli, D., Sommeria, J. & Lam, F.-P. A. 1997 Observation of an internal wave attractor in a confined stably-stratified fluid. *Nature* **388**, 557–561.

Maas, L. R. M. & Lam, F.-P. A. 1995 Geometric focusing of internal waves. *J. Fluid Mech.* **300**, 1–41.

Manders, A. M. M. & Maas, L. R. M. 2003 Observations of inertial waves in a rectangular basin with one sloping boundary. *J. Fluid Mech.* **493**, 59–88.

Manders, A. M. M. & Maas, L. R. M. 2004 On the three-dimensional structure of the inertial wave field in a rectangular basin with one sloping boundary. *Fluid Dyn. Res.* **35**, 1–21.

Matsuno, T. 1966 Quasi-geostrophic motions in the equatorial area. *J. Met. Soc. Japan II* **44**, 25–43.

McEwan, A. D. 1970 Inertial oscillations in a rotating fluid cylinder. *J. Fluid Mech.* **40**, 603–640.

Merzbacher, E. 1970 *Quantum Mechanics*, 2nd edn. Wiley & Sons.

Munk, W. 1980 Internal wave spectra at the buoyant and inertial frequencies. *J. Phys. Oceanogr.* **10**, 1718–1728.

Munk, W. & Phillips, N. A. 1968 Coherence and band structure of inertial motion in the sea. *Rev. Geophys.* **4**, 447–472.

Münnich, W. 1993 On the influence of bottom topography on the vertical structure of internal seiches. PhD thesis ETA Zürich.

Nedelec, J.-C. 2001 *Acoustic and Electromagnetic Equations*. Springer.

Ogilvie, G. I. 2005 Wave attractors and the asymptotic dissipation rate of tidal disturbances. *J. Fluid Mech.* **543**, 19–44.

Ogilvie, G. I. & Lin, D. N. C. 2004 Tidal dissipation in rotating giant planets. *Astrophys. J.* **610**, 477–509.

Ooyama, K. 1966 On the stability of baroclinic circular vortex: a sufficient crieterion for stability. *J. Atmos. Sci.* **23**, 43–53.

Rieutord, M., Georgeot, B. & Valdettaro, L. 2000 Wave attractors in rotating fluids: a paradigm for ill-posed Cauchy problems. *Phys. Rev. Lett.* **85**, 4277–4280.

Rieutord, M., Georgeot, B. & Valdettaro, L. 2001 Inertial waves in a rotating spherical shell: attractors and asymptotic spectrum. *J. Fluid Mech.* **435**, 103–144.

Rieutord, M. & Valdettaro, L. 1997 Inertial waves in a rotating spherical shell. *J. Fluid Mech.* **341**, 77–99.

Rieutord, M., Valdettaro, L. & Georgeot, B. 2002 Analysis of singular inertial modes in a spherical shell: the slender toroidal shell model. *J. Fluid Mech.* **463**, 345–360.

Stern, M. E. 1963 Trapping of low frequency oscillations in an equatorial 'boundary layer'. *Tellus* **15**, 246–250.

Stewartson, K. 1971 On trapped oscillations of a rotating fluid in a thin spherical shell. *Tellus* **23**, 506–510.

Stewartson, K. 1972 On trapped oscillations of a rotating fluid in a thin spherical shell II. *Tellus* **24**, 283–287.

Stewartson, K. & Rickard, J. A. 1969 Pathological oscillations of a rotating fluid. *J. Fluid Mech.* **5**, 577–592.

Stewartson, K. & Walton, I. C. 1976 On inertial oscillations in the oceans. *Tellus* **28**, 71–73.

Tilgner, A. 1999 Driven inertial oscillations in spherical shells. *Phys. Rev.* E **59**, 1789–1794.

Yavneh, I., McWilliams, J. C. & Molemaker, M. J. 2001 Non-axisymmetyric instability of centrifugally stable stratified Taylor-Couette flow. *J. Fluid Mech.* **448**, 1–21.

https://doi.org/10.1017/S0022112006002904 Published online by Cambridge University Press